CrystEngComm

Accepted Manuscript

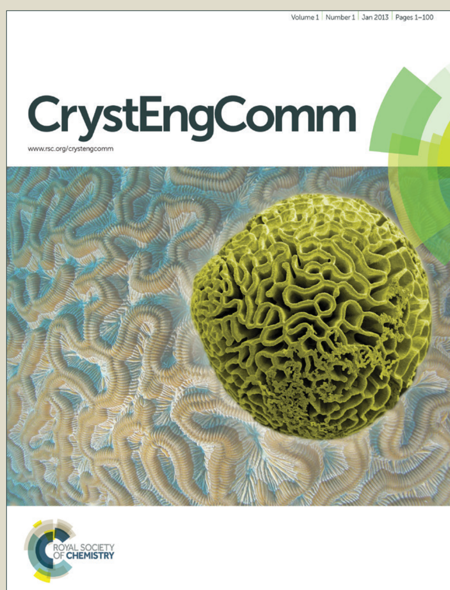

This is an *Accepted Manuscript*, which has been through the Royal Society of Chemistry peer review process and has been accepted for publication.

Accepted Manuscripts are published online shortly after acceptance, before technical editing, formatting and proof reading. Using this free service, authors can make their results available to the community, in citable form, before we publish the edited article. We will replace this *Accepted Manuscript* with the edited and formatted *Advance Article* as soon as it is available.

You can find more information about *Accepted Manuscripts* in the Information for Authors.

Please note that technical editing may introduce minor changes to the text and/or graphics, which may alter content. The journal's standard Terms & Conditions and the Ethical guidelines still apply. In no event shall the Royal Society of Chemistry be held responsible for any errors or omissions in this *Accepted Manuscript* or any consequences arising from the use of any information it contains.

ROYAL SOCIETY OF CHEMISTRY

www.rsc.org/crystengcomm

Journal Name
CrystEngComm
Dynamic Article Links ►
Cite this: DOI: 10.1039/c0xx00000x
www.rsc.org/xxxxxx
ARTICLE TYPE

Enhanced remnant polarization in ferroelectric $Bi_6Fe_2Ti_3O_{18}$ thin films

Dongpo Song,[a,b] Xuzhong Zuo,[a] Bing Yuan,[a] Xianwu Tang,[a] Wenhai Song,[a] Jie Yang,*[a] Xuebin Zhu,*[a] and Yuping Sun[a,b,c]

Received (in XXX, XXX) XthXXXXXXXXX 20XX, Accepted Xth XXXXXXXXX 20XX
DOI: 10.1039/b000000x

For the practical applications in ferroelectric memories, a large remnant polarization for nontoxic Pb-free ferroelectric materials is required. We prepared $Bi_6Fe_2Ti_3O_{18}$ thin films on Pt/Ti/SiO_2/Si (100) substrates by chemical solution deposition using different annealing processes, and found that a well-defined ferroelectric hysteresis loop with a rather large remnant polarization ($P_r \approx 21.5 \mu C/cm^2$) occurs in $Bi_6Fe_2Ti_3O_{18}$ thin films prepared by rapid thermal annealing in air. This value of remnant polarization is superior to that of other ferroelectric Aurivillius compounds such as Bi_2WO_6, Bi_3TiNbO_9, $Bi_4Ti_3O_{12}$, $Bi_5FeTi_3O_{15}$, and $Bi_6Fe_2Ti_3O_{18}$ thin films prepared by chemical solution deposition and pulsed laser deposition. The results of X-ray diffraction, high-resolution transmission electron microscopy, X-ray photoelectron spectroscopy and ferroelectric P-E hysteresis loops reveal that grain size, surface morphologies, oxygen vacancies and lattice distortion play very important roles in determination of the remnant polarization. The present study will provide an effective route to prepare the layered Aurivillius thin films with large remnant polarization by chemical solution deposition.

Introduction

Bismuth layered Aurivillius compounds with the general formula $(Bi_2O_2)^{2+}(A_{n-1}B_nO_{3n+1})^{2-}$ (A = Na, K, Ca, Sr, Ba, Pb, Bi, etc., and B = Ti, Fe, etc.) have a naturally-layered perovskite-related crystal structure which consist of perovskite-like $(A_{n-1}B_nO_{3n+1})^{2-}$ layers interleaved between fluorite-like $(Bi_2O_2)^{2+}$ layers, where the n refers to the numbers of the perovskite-like layers.[1-3] Aurivillius compounds with n = 2 and 3 are considered to be candidate materials for nonvolatile random access memory applications because of high fatigue-endurance ferroelectric properties, piezoelectric and environment-friendly (Pb-free) behaviours and so on.[4,5]

Recently, the Aurivillius-based materials have attracted renewed attention due to the potential candidates as room-temperature single-phase multiferroics by doping magnetic species at the B sites, especially for the n = 4 Aurivillius compound.[6,7] However, the obtained magnetic order is rather weak. It is suggested that a higher concentration of magnetic ions is desirable in order to achieve robust magnetic ordering above room-temperature.[8,9] One possible route to increase the concentration of magnetic ions is to focus on Aurivillius compounds with a higher number of perovskite-like layers, i.e., n > 4. Indeed, long-range magnetic ordering has been reported for several Aurivillius compounds with n = 5, i.e., $Bi_6Fe_2Ti_3O_{18}$ and $Bi_6Fe_{1.52}Mn_{0.68}Ti_{2.8}O_{18}$.[10,11] On the other hand, systematic investigations and optimization of the ferroelectric properties of the parent-compound are very important before doping magnetic species at Ti sites to explore single-phase multiferroics.[12,13] Moreover, for practical applications in ferroelectric memories, piezoelectric and multiferroic devices, thin films with a large remnant polarization (P_r) are required.[14]

Currently, investigations about improvement of ferroelectric polarization in $Bi_6Fe_2Ti_3O_{18}$ thin films are mainly focused on rare-earth substitution of Bi, higher-valence element doping at Ti and/or oxygen annealing process. Liu et al. found that the ferroelectric and ferromagnetic properties can be improved in Co-doped $Bi_6Fe_2Ti_3O_{18}$ thin films, in which the value of P_r can be increased from 10 $\mu C/cm^2$ for the undoped thin film to 17.6 $\mu C/cm^2$ for the $Bi_6Fe_{1.4}Co_{0.6}Ti_3O_{18}$.[15] The variation in P_r is attributed to the competition between the increased grain size and the oxygen vacancies duo to Co doping. Kim et al. reported that the V-doped $Bi_6Fe_2Ti_3O_{18}$ thin films exhibit the improved electrical and multiferroic properties by rapid thermal annealing under oxygen atmosphere.[16] The values of P_r is increased to 8.2 $\mu C/cm^2$ for the V-doped thin film as compared with 4 $\mu C/cm^2$ for the undoped $Bi_6Fe_2Ti_3O_{18}$ thin film, which is attributed to the reduced oxygen vacancies as well as the decreased mobility of oxygen vacancies by V doping. Additionally, a large P_r (18 $\mu C/cm^2$) is observed in the La and V co-doped $Bi_6Fe_2Ti_3O_{18}$ thin films although the hysteresis loops show leaky characteristics.[17] As mentioned above, the processing parameters are not quite same, which result in obvious differences in ferroelectric properties of the $Bi_6Fe_2Ti_3O_{18}$ thin film. Moreover, well-defined ferroelectric hysteresis loops with large P_r of $Bi_6Fe_2Ti_3O_{18}$ thin film is very crucial to obtain large magnetoelectric manipulations, which have not yet been achieved till now.

In this paper, we reported investigations about annealing processing effects of $Bi_6Fe_2Ti_3O_{18}$ thin films by chemical solution deposition (CSD). It was found that the value of P_r can be as high as 21.5 $\mu C/cm^2$ for the optimized $Bi_6Fe_2Ti_3O_{18}$ thin films, which

CrystEngComm Accepted Manuscript

will provide a facile route to enhance the ferroelectric properties in aurivillius-based thin films.

Experimental

$Bi_6Fe_2Ti_3O_{18}$ (BFTO) thin films were prepared on polycrystalline Pt/Ti/SiO_2/Si (100) substrates by chemical solution deposition. The precursor solution was prepared using bismuth (III) acetate [$Bi(CH_3COO)_3$], iron (II) acetate [$Fe(CH_3COO)_2$], and tetrabutyl titanate [$Ti(OC_4H_9)_4$] as starting materials and propionic acid [CH_3CH_2COOH] as solvent. Details of the solution preparation and spin coating processing are described in our previous work.[18] BFTO thin films were subsequently crystallized by two thermal annealing processes, i.e., rapid thermal annealing (RTA, i.e., simply inserting the thin films into the furnace at the final annealing temperature) and slow thermal annealing (STA, heating rate of 10 °C /min). For each thermal annealing processing, BFTO thin films were annealed under nitrogen, air, and oxygen atmospheres at 700°C for 0.5 h. For the sake of simplicity, the thin films prepared under nitrogen atmosphere by STA is defined as N-STA. Analogically, other samples are labelled as N-RTA, A-STA, A-RTA, O-STA and O-RTA, where N, A and O denotes that the annealing atmosphere is nitrogen, air and oxygen, respectively.

The crystal structure was determined by a Philips X'Pert PRO X-ray diffractometer (XRD) with Cu-K_α radiation at room-temperature. The microstructures were checked up by a field emission scanning electron microscopy (FE-SEM, Sirion 200, FEI Company, USA). The energy dispersive X-ray (EDX) analysis spectra were also carried out in the field emission scanning electron microscopy to obtain the stoichiometry. High-resolution transmission electron microscopy (HRTEM) images and selected area electron diffraction (SAED) patterns were performed using a JEM-2010 transmission electron microscope (JEM-2010, JEOL Ltd., Japan) to give a more detailed crystal structures. The measurements of X-ray photoelectron spectroscopy (XPS, VG Scientific, ESCALAB250, USA) were done by using Al K_α to obtain information about the valence state. The ferroelectric properties were measured using a Sawyer-Tower circuit attached to a computer-controlled standardized ferroelectric test system (Precision Premier II, Radiant Technology, USA).

Results and discussion

Figure 1(a) shows the room-temperature XRD patterns of all derived BFTO thin films, and the inset shows the crystal structure of a half orthorhombic unit cell of BFTO. As shown in Fig. 1(a), it is seen that all the samples are phase-pure with a random orientation and can be indexed with an orthorhombic lattice with the space group *B2cb*, which is consistent with the previous results.[15, 18] It is noticed that the XRD patterns of all BFTO films annealed in nitrogen, air and oxygen show the analogous characteristics, indicating that the phase formation is not seriously affected by the annealing atmosphere in this experiment. Due to the similar XRD results for Aurivillius structure with near $(A_{n-1}B_nO_{3n+1})^{2-}$ layers, HRTEM measurements are carried out to further confirm the crystal structure of the derived thin films. As shown in Fig. 1(b) and (c) of the HRTEM and Fourier transform results for the A-RTA thin film respectively, it is clearly seen a stack structure with 5-layered perovskite-like layers sandwiched by two fluorite-like $(Bi_2O_2)^{2+}$ layers is formed, which is also confirmed by the SAED pattern as shown in Fig. 1(d) and is analogous to the results in other Aurivillius compounds.[7,11,19] The c-axis lattice constant *c* of the A-RTA thin film is measured to be 4.9356(1) nm, which is close to the value obtained from XRD result.

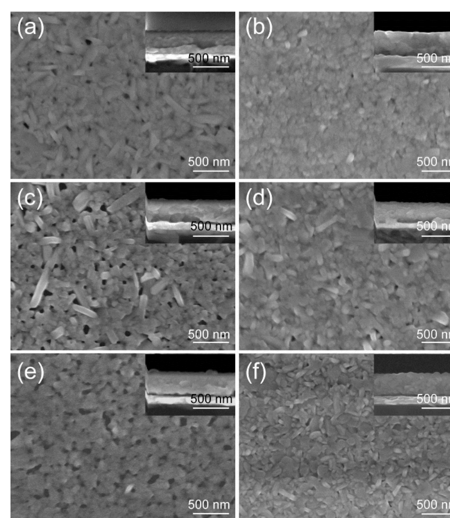

Fig. 2 Surface FE-SEM results for all derived $Bi_6Fe_2Ti_3O_{18}$ thin films (a) N-STA, (b) N-RTA, (c) A-STA, (d) A-RTA, (e) O-STA and (f) O-RTA. The corresponding insets are the cross-section FE-SEM results to give the thickness.

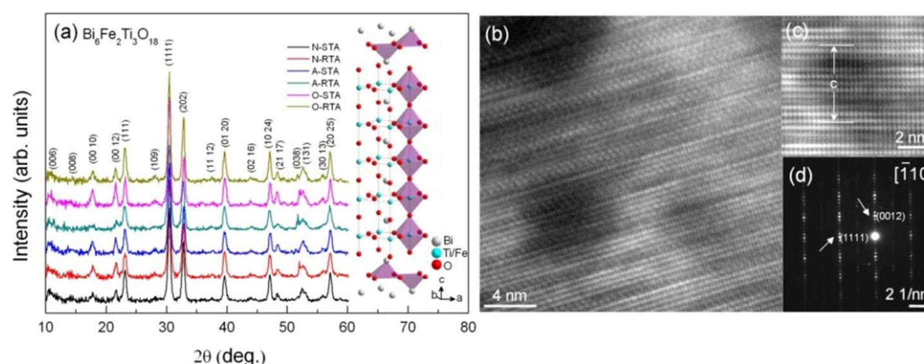

Fig. 1 XRD patterns of all derived $Bi_6Fe_2Ti_3O_{18}$ thin films (a) and HRTEM image of A-RTA thin film (b). The inset (a) shows the lattice structure of a half orthorhombic unit cell.(c) The HRTEM microstructural analysis image by the Fourier transform and the inverse transform, it is clearly seen a stack structure with 5-layered perovskite-like layers sandwiched by two fluorite-like $(Bi_2O_2)^{2+}$ layers is formed. (d) SAED pattern of the thin film.

CrystEngComm Accepted Manuscript

This journal is © The Royal Society of Chemistry [year]

The surface FE-SEM results for all derived thin films are shown in Fig. 2. It is seen that the thin films annealed by the RTA processing are denser than these by the STA processing despite of the annealing atmosphere. The enhanced density can be attributed to two facts that high heating rate will delay the crystallization to higher temperatures and the retained a lower viscosity structure to higher temperatures.[20] Additionally, the BFTO thin films annealed in air have a larger particle size compared with those annealed in N_2 and O_2. On the other hand, plate-like grains are usually observed for ceramic samples and thin films due to the anisotropic nature of the crystal structure of the Aurivillius phase materials.[21] However, in this experiment grain-like morphologies appearance in the derived thin films can be attributed to the lower annealing temperature as compared to that of the ceramics. In turn, this characteristic of morphologies may endow enhanced ferroelectric properties as discussed below because of the polarization anisotropy.[5] Thickness of all derived BFTO thin films is almost the same as 450 nm obtained by the cross-section FE-SEM results as shown in the corresponding insets of Fig. 2.

Fig. 3(a) shows the room-temperature ferroelectric polarization hysteresis loops (P-E). It is seen that all the derived BFTO thin films show a well-defined ferroelectric hysteresis loop under the maximum applied electric field up to 670 kV/cm, which is obviously different with the previous result, in which it shows no remanent polarization or highly leaky characteristics.[17] Notably, the A-RTA thin film exhibits an enhanced hysteresis-loop squareness and the remnant polarization P_r reaches as high as 21.5 μC/cm^2. To the best of our knowledge, this value is superior to the P_r of other ferroelectric Aurivillius compounds such as Bi_2WO_6, Bi_3TiNbO_9, $Bi_4Ti_3O_{12}$, $Bi_5FeTi_3O_{15}$, and $Bi_6Fe_2Ti_3O_{18}$ thin films prepared by chemical solution deposition and pulsed laser deposition.[7,16,22,23] Furthermore, the P_r is comparable to those of the rare-earth-substituted $Bi_4Ti_3O_{12}$ thin films, which have been extensively investigated as candidates for the lead-free ferroelectrics and components of nonvolatile FRAM.[5]

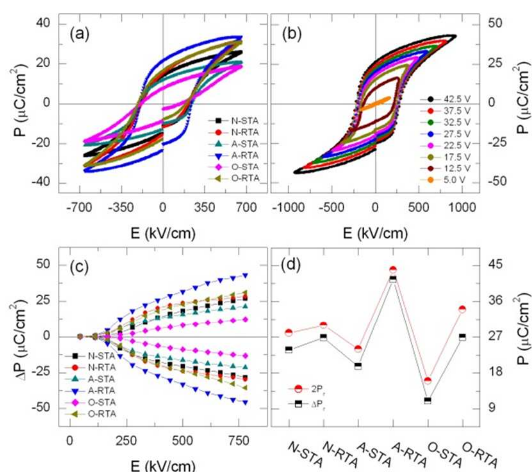

Fig. 3 Ferroelectric hysteresis loops of $Bi_6Fe_2Ti_3O_{18}$ thin films measured at room-temperature with 5 kHz frequency. (a) P-E hysteresis loops of all samples, (b) P-E hysteresis loops of the A-RTA sample measured under different applied electric fields. (c) PUND results for all samples at different applied electric field and (d) the variation of ΔP and $2P_r$ for all derived BFTO thin films under different thermal annealed processes.

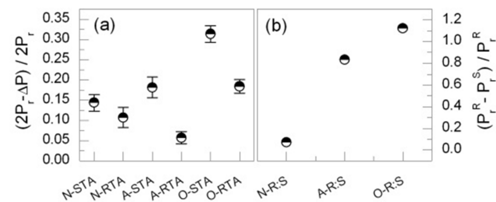

Fig. 4 $(2P_r - \Delta P) / 2P_r$ and $(P_r^R - P_r^S) / P_r^R$ *vs.* different annealing process.

In order to give a clearly image of polarization responded on the applied electric field, ferroelectric tests under different applied electric fields were carried out. Fig. 3(b) shows the P-E hysteresis loops measured at different applied electric fields for the A-RTA thin film, and the other thin films have the analogous characteristics in polarization, that means the P_r increases with increasing electric field. The P_r value measured at the maximum applied electric field of 945 kV/cm can be as 26.1 μC/cm^2 and a well-defined P-E hysteresis loop can be obtained when the applied electric field reach as 333 kV/cm as shows in Fig. 3(b).

To evaluate the contribution of leakage current to the P_r, we performed the measurements of a positive-up negative-down (PUND) pulsed polarization and the polarization can be defined as $\Delta P = P^*$ (switched polarization) − $P^\wedge$ (nonswitched polarization).[24,25] The electric field dependence of ΔP is shown in Fig. 3(c). To compare the P-E hysteresis-loop and PUND results, we choose the values of ΔP and $2P_r$ under the same applied electric field (670 kV/cm) and plot the variation in ΔP and $2P_r$ for the BFTO thin films under different processing as shown in Fig. 3(d). It is seen that all the values of ΔP are comparable with the $2P_r$, implying that the influence of the leakage current contribution on the remnant polarization is insignificant. In order to give a clear image of extrinsic contributions (mainly leakage current), the value of $(2P_r - \Delta P) / 2P_r$ are plot in Fig. 4(a), it can be seen that the A-RTA sample exhibits the lowest value 0.057 as compared to that of 0.314 in the O-STA sample. The tendencies can be attributed to different oxygen vacancies and bismuth content in the derived thin films as discussed below.

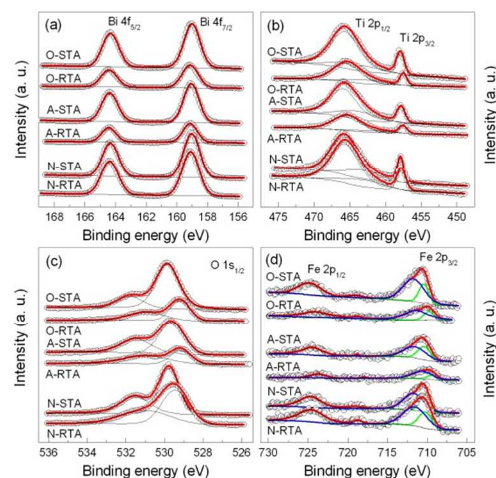

Fig. 5 XPS spectra of $Bi_6Fe_2Ti_3O_{18}$ thin films. (a) Bi 4*f*, (b) Ti 2*p*, (c) O 1*s*, (d) Fe 2*p* and deconvoluted results. The blue and green line in (d) represent to Fe^{3+} and Fe^{2+} fitting peak.

From Fig. 3(d), one can also see that the ferroelectric polarization of thin films prepared by RTA is larger than that prepared by STA under the same atmosphere. Due to the

CrystEngComm Accepted Manuscript

suppressed Bi volatilization in RTA processing, it is conjectured that the Bi vacancies dominate the variation in ferroelectric polarization of the derived BFTO thin films.[26] However, as shown in Fig. 4(b) the ratio of $(P_r^R - P_r^S) / P_r^R$ (where P_r^R and P_r^S represents remnant polarization of RTA and STA process, respectively) is only 0.07 in N_2 atmosphere as compared to the value of 1.125 in O_2 atmosphere, which indicates that the volatility of bismuth are different under different atmospheres and some other factors should be considered. On the other hand, it is suggested that ferroelectric thin films prepared under oxygen atmosphere will suppress the formation of oxygen vacancies, which will give rise to the increased ferroelectric polarization.[27] Therefore, it is suggested that the O-RTA thin film should possess the minimum oxygen vacancies as well as the maximum ferroelectric polarization among all BFTO thin films. In fact, the maximum ferroelectric polarization among all the derived BFTO thin films is attributed to the thin film A-RTA, which suggests that some additional factors should be considered. Additionally, the larger particle size in BFTO thin films prepared under air atmosphere is beneficial for the increased remnant polarization, however, the subtle changes in grain size cannot account for the obvious variation in remnant polarization. Moreover, all BFTO thin films show a random orientation, which can rule out the influence of films orientation on ferroelectric polarization. To the best of our knowledge, the factors influencing ferroelectric polarization in the higher *n* Aurivillius ferroelectric compounds are not completely clear yet, although the origin of ferroelectric polarization in perovskite-type ferroelectrics such as $BiFeO_3$, $BaTiO_3$, $PbTiO_3$ has already extensively reported to date.[29,30] Three main factors including oxygen vacancies (ions valence variation and defect centres), Bi vacancies (Bi 6s lone pair), and lattice distortion (ions displacement and octahedral rotation) are suggested to play important roles in determination of the ferroelectric polarization in BFTO thin films with a Aurivillius structure. With this notion in mind, we check the above-mentioned three factors to figure out why the A-RTA thin film has the maximum ferroelectric polarization among all BFTO thin films.

XPS measurements were carried out to obtain more information about element valence in the derived BFTO thin films. Fig. 5(a) illustrates the Bi 4*f* core-level spectra of all derived BFTO thin films. The peaks located at the range of 158.98 - 159.08 eV and 164.28 - 164.48 eV can be attributed to the Bi $4f_{7/2}$ (158.60 eV) and Bi $4f_{5/2}$ (163.99) in Bi_2O_3, respectively.[30] The core-level spectra of Ti 2*p* in BFTO are shown in Fig. 5(b). The spin-orbit splitting Ti $2p_{1/2}$ and Ti $2p_{3/2}$ peaks located at around 465.68 and 457.98 eV, respectively, are corresponding to the binding energy of Ti $2p_{1/2}$ (464.7 eV) and Ti $2p_{3/2}$ (458.2 eV) in TiO_2.[31] The core-level spectra for all derived thin films displayed in Fig. 5(a) and (b) are almost indiscriminate with each other. Fig. 5(c) shows the results of the O 1*s* peaks of all the derived BFTO thin films. It is seen that the O 1*s* XPS peak can be deconvoluted into two peaks, with the binding energy of 529.68 and 530.68 eV, respectively. The former one can be assigned to the O^{2-} ions in the crystal structure that is the lattice oxygen.[32] The peak with higher binding energy at 531.68 eV is attributed to the near-surface oxygen. It should be noted that the Ti 2*p* and O 1*s* core-level spectra of the thin films prepared by RTA processing shift obviously to lower binding energy as compared with the thin films by STA processing except for the thin films annealed under nitrogen atmosphere. In other words, the XPS spectra is less susceptible for the samples annealed under nitrogen atmosphere by RTA and STA process, which is also reflected from the subtle changes in P_r. Fig. 5(d) shows the Fe 2*p* core-level spectra and the deconvoluted curves taking into account of the contribution of both Fe^{2+} and Fe^{3+} ions. Taking the XPS spectra of the A-RTA thin film as an example, the binding energy of Fe $2p_{1/2}$ and Fe $2p_{3/2}$ peaks located at around the binding energy of 709.36 and 710.75 eV, respectively, is very close to that of the Fe^{2+} $2p_{1/2}$ (709.00 eV) in Fe_3O_4 and Fe^{3+} $2p_{3/2}$ (710.80 eV) in Fe_2O_3, respectively.[33] In this case, the oxygen vacancies will be induced to maintain the charge neutrality when Fe^{3+} reduces to Fe^{2+} through the Kröger-Vink relation:

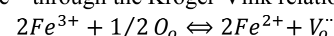

$$2Fe^{3+} + 1/2\, O_o \Leftrightarrow 2Fe^{2+} + V_o^{\cdot\cdot}$$

O_o represents the null oxygen, $V_o^{\cdot\cdot}$ represents the oxygen vacancy with two positive charges. We can estimate roughly the percentage of oxygen vacancies in all derived BFTO thin films by calculating the relative area ratio under the curves of deconvoluted Fe^{2+} and Fe^{3+} peaks.[34] Fig. 6(a) and (b) show the variation of P_r and oxygen vacancies prepared by different processing, respectively. One can clearly see that the relationship between the P_r and the oxygen vacancies is almost mirror symmetric, implying that the oxygen vacancies may contribute dominantly to the P_r. It is known that oxygen vacancies tend to drift and aggregate at domain walls and block the domain switching, which will give rise to deterioration of the remnant polarization.[27] However, if the oxygen vacancies is dominant in determination of the P_r, the values of P_r in the oxygen-annealed thin films should be higher than those in the nitrogen-annealed thin films since the oxygen-annealed thin films have a relatively lower amount of oxygen vacancies, which is different with the experimental results.

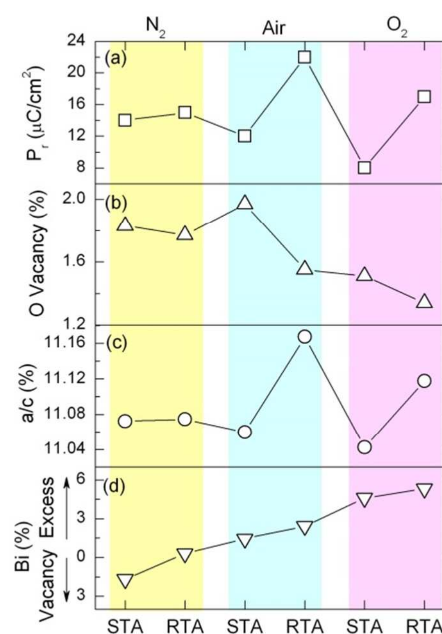

Fig. 6 Remnant polarization, oxygen vacancies, lattice distortion and bismuth vacancies in the $Bi_6Fe_2Ti_3O_{18}$ thin films according to atmosphere and annealing process used.

This journal is © The Royal Society of Chemistry [year]

CrystEngComm Accepted Manuscript

It is known that the lattice distortion can also affect the ferroelectric polarization for the displacement ferroelectrics because of the crystal anisotropy of the ferroelectric phase in perovskite ferroelectrics such as $BiFe_3O_{12}$, $PbTiO_3$ and $BaTiO_3$.[29,30] Moreover, Chon *et al.* also pointed out that the off-centre displacements (i.e., the lattice distortion) of the central Ti ion adjacent to the interleaving Bi_2O_2 layer is the main contribution to the large spontaneous polarization in the layered Aurivillius compound $Bi_{4-x}Nd_xTi_3O_{12}$.[22] Accordingly, we can estimate the relative magnitude of lattice distortion in BFTO thin films by the ratio of the polar axis to the nonpolar axis, i.e., *a*/*c*, as shown in Fig. 6(c). The lattice distortion in the derived BTFO thin films can be attributed to different residual microstrain in the derived thin films due to different processing parameters.[35,36] One can see that both the trend and the magnitude of variation in the *a*/*c* are in good agreement with the tendencies in P_r. The Bi vacancies were determined by EDX measurements and the results are shown in Fig. 6(d). Taking into account of both the trend and the magnitude of variation in P_r, the oxygen vacancies, the Bi vacancies and the lattice distortion, one can make a conclusion that the factors of the oxygen vacancies and lattice distortion are dominant for the nitrogen-, and air-annealed thin films. On the other hand, the P_r for the oxygen-annealed thin films implying that the Bi excess may play a more critical role in P_r for the oxygen-annealed thin films. For the A-RTA thin films, it seems that the larger grain size, compact surface morphologies, and relatively larger lattice distortion are beneficial to the maximum P_r.

Conclusions

In summary, the structural and the ferroelectric properties of $Bi_6Fe_2Ti_3O_{18}$ thin films by different thermal annealing processes were studied. All the derived samples are determined to be typical 5-layered Aurivillius structure at room temperature. The thin films prepared by rapid thermal annealing show a superior ferroelectricity to the samples prepared by slow thermal annealing in the same atmosphere. The thin film prepared by rapid thermal annealing under air atmosphere shows the largest remnant polarization of 21.5 μC/cm^2 due to the larger grain size, the more compact surface morphology and the relatively larger lattice distortion. The present study will provide an effective route to prepare the layered Aurivillius thin films with large remnant polarization by chemical solution deposition.

This work was supported by the National Natural Science Foundation of China (Grant No. 11274313, 11204316), the Anhui Provincial Natural Science Foundation (Grant No. 1208085MA06), and the Joint Funds of the National Natural Science Foundation of China and the Chinese Academy of Sciences' Large-Scale Scientific Facility (Grant No. U1232138, U1232210, and U1432137). It was also sponsored by the Scientific Research Foundation for the Returned Overseas Chinese Scholars, State Education Ministry. Y. P. Sun acknowledges support by the National Key Basic Research (Grant No. 2011CBA00111).

Notes and references

[a]Key Laboratory of Materials Physics, Institute of Solid State Physics, Chinese Academy of Sciences, Hefei 230031, People's Republic of China; E-mail: jyang@issp.ac.cn, xbzhu@issp.ac.cn
[b]University of Science and Technology of china, Hefei 230026, People's Republic of China
[c]High Magnetic Field Laboratory, Chinese Academy of Sciences, Hefei 230031, People's Republic of China

1 E. C. Subbarao, J. Phys. Chem. Solids, 1962, **23**, 665-676.
2 X. Z. Zuo, J. Yang, B. Yuan, D. P. Song, X. W. Tang, K. J. Zhang, X. B. Zhu, W. H. Song, J. M. Dai and Y. P. Sun, RSC Adv., 2014, **4**, 46704-46709.
3 S. J. Sun, G. P. Wang, J. L. Wang, Z. P. Fu, R. R. Peng, R. J. Knized and Y. L. Lu, Nanoscale, 2014, **6**, 13494-13500.
4 C. A. P.Dearaujo, J. D. Cuchiaro, L. D. Mcmillan, M. C. Scott and J. F. Scott, Nature, 1995, **374**, 627-629.
5 H. N. Lee, D. Hesse, N. Zakharov and U. Gosele, Science, 2002, **296**, 2006-2009.
6 X. Mao, W. Wang, X. Chen and Y. Lu, Appl. Phys. Lett., 2009, **95**, 082901.
7 H. Y. Zhao, H. Kimura, Z. X. Cheng, M. Osada, J. L. Wang, X. L. Wang, S. X. Dou, Y. Liu, J. D. Yu, T. Matsumoto, T. Tohei, N. Shibata and Y. Ikuhara, Sci. Rep., 2014, **4**, 5255.
8 A. Y. Birenbaum and C. Ederer, arXiv: 1407.3973, 2014.
9 S. J. Sun, Y. H. Ling, R. R. Peng, M. Liu, X. Y. Mao, X. B. Chen, R. J. Knize and Y. L. Lu, RSC Adv., 2013, **3**, 18567-18572.
10 E. Jartych, T. Pikula, M. Mazurek, A. Lisinska-Czekaj, D. Czekaj, K. Gaska, J. Przewoznik, C. Kapusta and Z. Surowiec, J. Magn. Magn. Mater., 2013, **342**, 27-34.
11 L. Keeney, T. Maity, M. Schmidt, A. Amann, N. Deepak, N. Petkov, S. Roy, M. E. Pemble and R. W. Whatmore, J. Am. Ceram. Soc., 2013, **96**, 2339-2357.
12 J. Wang, J. B. Neaton, H. Zheng, V. Nagarajan, S. B. Ogale, B. Liu, D. Viehland, V. Vaithyanathan, D. G. Schlom, U. V. Waghmare, N. A. Spaldin, K. M. Rabe, M. Wuttig and R. Ramesh, Science, 2003, **299**, 1719-1722.
13 B. Yuan, J. Yang, J. Chen, X. Z. Zuo, L. H. Yin, X. W. Tang, X. B. Zhu, J. M. Dai, W. H. Song and Y. P. Sun, Appl. Phys. Lett., 2014, **104**, 062413.
14 N. Setter, D. Damjanovic, L. Eng, G. Fox, S. Gevorgian, S. Hong, A. Kingon, H. Kohlstedt, N. Y. Park, G. B. Stephenson, I. Stolitchnov, A. K. Taganstev, D. V. Taylor, T. Yamada and S. Streiffer, J. Appl. Phys., 2006, **100**, 051606.
15 Z. Liu, J. Yang, X. W. Tang, L. H. Yin, X. B. Zhu, J. M. Dai and Y. P. Sun, Appl. Phys. Lett., 2012, **101**,122402.
16 H. J. Kim, J. W. Kim, E. J. Kim, J. Y. Choi, C. M. Raghavan, W. J. Kim, M. H. Kim, T. K. Song, J. W. Kim and S. S. Kim, Ferroelectrics, 2014, **465**, 68-75.
17 C. M. Raghavan, J. W. Kim and S. S. Kim, Ceram. Int., 2014, **40**, 10649-10655.
18 D. P. Song, X. W. Tang, B.Yuan, X. Z. Zuo, J. Yang, L.Chen, W. H. Song, X. B. Zhu and Y. P. Sun, J. Am. Ceram. Soc., 2014, **97**, 3857-3863.
19 J. L. Wang, Z. P. Fu, R. R. Peng, M. Liu, S. J. Sun, H. L. Huang, L. Li, R. J. Knize and Y. L. Lu**,** Mater. Horiz., 2015, 10.1039/C4MH00202D.
20 R. W. Schwartz, Chem. Mater., 1997, **9**, 2325-2340.
21 C. Q. Long, H. Q. Fan, M. M. Li, P. R. Ren and Y. Cai, CrystEngComm, 2013, **15**, 10212-10221.
22 U. Chon, H. Jang, M. Kim and C. Chang, Phys. Rev. Lett., 2002, **89**,087601.
23 B. Yang, X. J. Zhang, S. T. Zhang, X. Y. Chen, Y. F. Chen, Y. Y. Zhu, Z. G. Liu and N. B. Ming, Ferroelectrics, 2001, **525**, 281-288.
24 S. J. Sun, Y. H. Ling, R. R. Peng, M. Liu, X. Y. Mao, X. B. Chen, R. J. Knize and Y. L. Lu, RSC Adv.,2013, **3**, 18567-18572.
25 X. W. Tang, L. Hu, J. Yang, L. Chen, J. M. Dai, W. H. Song, Z. R. Yang, X. B. Zhu and Y. P. Sun, RSC Adv., 2014, **4**, 32738-32743.
26 J. B.Neaton, C. Ederer, U. V. Waghmare, N. A. Spaldinand and K. M. Rabe, Phys. Rev. B, 2005, **71**, 014113.
27 J. F. Scott and C. A. P. Dearaujo, Science, 1989, **246**, 1400-1405.

CrystEngComm Accepted Manuscript

28 J. X. Zhang, Q. He, M. Trassin, W. Luo, D. Yi, M. D. Rossell, P. Yu, L. You, C. H. Wang, C. Y. Kuo, J. T. Heron, Z. Hu, R. J. Zeches, H. J. Lin, A. Tanaka, C. T. Chen, L. H. Tjeng, Y. H. Chu and R. Ramesh, Phys. Rev. Lett., 2011, **107**, 147602.

29 R. E. Cohen, Nature, 1992, **358**, 136-138.

30 Y. Schuhl, H. Baussart, R. Delobel, M. L. Bras, J. Leroy, L. G. Gengembre, and J. Rimblot, J. Chem. Soc. Faraday Trans.1, 1983, **79**, 2055-2069.

31 K. Y. Yang, K. Z. Fung, and M. C. Wang, J. Appl. Phys., 2006, **100**, 056102.

32 A. Tamilselvan, S. Balakumar, M. Sakar, C. Nayek, P. Murugavel and K. S. Kumar, Dalton Trans., 2014, **43**,5731-5738.

33 B. J. Tan, K. J. Klabunde and P. M. A. Sherwood, Chem. Mater., 1990, **2**, 186-191.

34 S. F. Liu, Y. J. Wu, J. Li and X. M. Chen, Appl. Phys. Lett., 2014, **104**, 082912.

35 W. Qin, T. Nagase, Y. Umakoshi and J. A. Szpunar, Philo. Mag. Lett., 2008, **88**, 169-179.

36 P. S. V. Mocherla, C. Karthik, R. Ubic, M. S. R. Rao and C. Sudakar, Appl. Phys. Lett., 2013, 103, 022910.

CrystEngComm Accepted Manuscript

This journal is © The Royal Society of Chemistry [year]